Collision-Energy-Resolved Penning Ionization Electron Spectroscopy of Toluene and Chlorotoluenes : Stereodynamics in Collisional Ionization and Anisotropic Interactions with He*(23S) atoms

doi: 10.1140/epjd/e2005-00269-3

Eur. Phys. J. D **38**, 75–84 (2006)
DOI: 10.1140/epjd/e2005-00269-3

THE EUROPEAN PHYSICAL JOURNAL D

Collision-energy-resolved Penning ionization electron spectroscopy of toluene and chlorotoluenes

Stereodynamics in collisional ionization and anisotropic interactions with $He^*(2^3S)$ atoms

N. Kishimoto, M. Matsumoto, E. Matsumura, and K. Ohno[a]

Department of Chemistry, Graduate School of Science, Tohoku University, Aoba-ku, Sendai 980-8578, Japan

Received 27 July 2005 / Received in final form 7 September 2005
Published online 4 October 2005 –

Abstract. Stereodynamics in ionization of toluene and *o*-, *p*-chlorotoluenes by collision with $He^*(2^3S)$ metastable atoms were investigated by two-dimensional collision-energy/electron-energy-resolved Penning ionization electron spectroscopy. Anisotropic interactions around the molecule were studied by the collision energy dependence of partial ionization cross-sections (CEDPICS) as well as model potential calculations, and shielding effect by the methyl group was observed in CEDPICS for ionization from Cl lone-pair orbitals of *o*-chlorotoluene. Attractive interaction with $He^*(2^3S)$ around the π orbital region was found to be larger for toluene rather than *o*-, *p*-chlorotoluenes. Exterior electron density (EED) calculation of partial ionization cross-sections in Penning ionization and negative CEDPICS for ionization band observed in ca. 4 eV in electron energy indicated that $\pi^{-2}\pi^{+1}$ shake-up state was observed in Penning ionization electron spectroscopy of toluene.

PACS. 34.20.-b Interatomic and intermolecular potentials and forces, potential energy surfaces for collisions – 34.20.Gj Intermolecular and atom-molecule potentials and forces – 34.50.Lf Chemical reactions, energy disposal, and angular distribution, as studied by atomic and molecular beams

1 Introduction

In the case of chemical reaction induced by collision between neutral species, it can be important for obtaining information on stereodynamics around the local part of molecules to compare reactivity and its collisional energy dependence for structural isomers containing the same functional groups.

A chemiionization process known as Penning ionization [1–3] can occur when a metastable excited atom A^* collides with a target molecule (or atom) M, where A^* has larger excitation energy than the lowest ionization potential (IP) of M:

$$M + A^* \rightarrow M^+ + A + e^-. \quad (1)$$

Two important variables of the Penning ionization process, (a) collision energy E_c between A^* and M in the entrance channel of the reaction and (b) kinetic energy E_e of the ejected electrons in the exit channel, can be measured by (A) velocity (or collision energy) selection of A^* and (B) Penning ionization electron spectroscopy (PIES) [4,5], respectively. When one measures a total Penning ionization cross-section as a function of the collision energy, it is difficult to obtain information on stereodynamics of the reaction around a local part of the target molecule M because the total ionization cross-section is the sum of partial ionization cross-sections and, therefore, it reflects averaged characteristics of the interaction [6–11]. Ionic-state-resolved partial Penning ionization cross-sections as a function of collision energy [12,13] and collision-energy-resolved Penning ionization electron spectra (CERPIES) [14,15] can be measured by collision-energy/electron-energy-resolved two dimensional Penning ionization electron spectroscopy (2D-PIES) [16] that is the combined technique of the methods (A) and (B).

In the Penning ionization process, an electron exchange model [17] was proposed for the reaction mechanism: an electron in a molecular orbital (MO) is transferred to the inner-shell orbital of colliding A^*, and the excited electron in A^* is ejected into the continuum. It has been shown from the study of $He^*(2^3S)$ PIES that the most effective geometrical situations for the Penning ionization are different depending upon the electron distribution of the target MOs [18]. For quantitative estimate of relative band intensity in PIES, an exterior electron density was calculated using ab initio molecular orbital wave functions [18,19]. In the exterior electron density model, exterior electron densities (EED) are defined for individual MOs

$$(\mathrm{EED})_i = \int_\Omega |\varphi_i(r)| \mathrm{d}r \quad (2)$$

[a] e-mail: ohnok@qpcrkk.chem.tohoku.ac.jp

where Ω is the subspace outside the boundary surface and φ_i is the respective MO to be ionized. Calculated EED values have been found to be in good agreement with the observed band intensities of $He^*(2^3S)$ PIES, that is reactivity of each MO with A^*, where the boundary surface was approximated by rigid van der Waals spheres [18,19].

Since the electron distribution of valence MOs is more or less localized around the boundary surface of the collision, the measurement of collision energy dependence of partial ionization cross-sections (CEDPICS) [12,14] for ionization from MOs enables us to investigate the local information on interaction potentials. Attractive interactions between M and $He^*(2^3S)$ were found for the out-of-plane directions of a benzene ring [15,20,21], while repulsive interactions were found for σ_{CH} orbital region. On the other hand, the interaction around the halogen atom is highly anisotropic. In the case of Cl atom, the interaction potential for a collinear direction approach of He^* to the C–Cl bond of CH_2=CHCl [22], C_2H_5Cl [23], and C_6H_5Cl [24] is less attractive than that for perpendicular directions of the C–Cl bond.

For a chlorotoluene molecule, attractive interactions are expected around the Cl atom and the phenyl ring, while repulsive interaction around the methyl group may shield the attractive interaction around the Cl atom. The orbital reactivities of chlorotoluenes including ortho, meta, and para isomers were previously [25] studied by $He^*(2^3S)$ PIES band intensities. In this study, we investigate stereodynamics and the anisotropic interaction potential between $He^*(2^3S)$ and chlorotoluene isomers by 2D-PIES. Anisotropic interactions around the Cl atom or the benzene ring and the effect in interaction potentials caused by the substitution groups are discussed.

2 Experiment

The experimental apparatus for He I UPS and $He^*(2^3S)$ 2D-PIES has been reported previously [16,26,27]. Metastable $He^*(2^3S, 2^1S)$ atoms were produced by a discharge nozzle source with a tantalum hollow cathode. $He^*(2^1S)$ components were quenched by a helium dc lamp. He I resonance photons (584 Å, 21.22 eV) produced by a discharge in pure helium gas were used for photoelectron spectroscopy. The kinetic energy of the electrons ejected in Penning ionization or photoionization were determined by a hemispherical electronic deflection type analyzer at a collection angle of 90° with respect to the incident He^* or photon beam. The energy resolution of the electron energy analyzer was estimated to be 60 meV from the full width at half-maximum of $Ar^+(^2P_{3/2})$ peak in the He I UPS. The transmission of the electron energy analyzer was determined by comparing our UPS data with those by Gardner and Samson [28] and Kimura et al. [29].

For the collision-energy-resolved/electron-energy-resolved two-dimensional measurement, the He^* beam was modulated by a pseudorandom chopper [30] rotating ca. 400 Hz and introduced into a reaction cell at 504 mm downstream from the pseudorandom chopper. Time dependent electron signals for each electron kinetic energy E_e were measured with a dwell time of 3 μs and recorded with scanning electron energies of 35 meV step. In order to obtain higher electron counts, we lowered the resolution of the analyzer to 250 meV in the 2D measurements. The time-of-flight (TOF) spectrum of $He^*(2^3S)$ was obtained by detecting signals of electrons emitted from a stainless steel plate inserted at the center of the reaction cell. The CEDPICS were obtained from 2D data within an appropriate range of E_e (typically the fwhm of the respective band) to avoid the effect of neighboring bands.

3 Calculations

For a discussion about UPS and PIES bands, we performed ab initio self-consistent field (SCF) calculations in order to obtain electron density contour maps and schematic diagrams of respective MOs. The geometrical parameters of the target molecules were optimized by density functional hybrid method (B3LYP) [31] using 6-311+G* basis set.

The electron density maps were calculated with 6-311++G** basis set and shown on the molecular plane for a' MOs and those of a'' orbitals are plotted on a plane above 1.7 Å (van der Waals radii of C) from the molecular plane. In electron density contour maps reported in the figures, thick solid curves indicate the repulsive molecular surface approximated by van der Waals radii [32] (r_C = 1.7 Å, r_H = 1.2 Å, and r_{Cl} = 1.95 Å). Schematic diagrams of MOs indicating component atomic orbitals were calculated with 4-31G basis set and shown by circles and ellipses. Solid circles showed valence s orbitals, where couples of ellipses and dashed circles showed in-plane and out-of-plane components of p orbitals, respectively. Signs of orbital coefficients were indicated by the thickness of the lines. Calculations of EED values outside the van der Waals surface were performed using the SCF MOs by 6-311++G** basis set. The IP values were calculated by the outer valence Green's function (OVGF) method [33] with cc-pVTZ basis set.

Interaction potentials between $He^*(2^3S)$ and the target molecule in various directions were calculated on the basis of the well-known resemblance between $He^*(2^3S)$ and $Li(2^2S)$ [34]; the shape of the velocity dependence of total scattering cross-section of $He^*(2^3S)$ by He, Ar, and Kr is similar to that of $Li(2^2S)$, and the location of the interaction potential well and its depth are similar for $He^*(2^3S)$ and $Li(2^2S)$ with various targets [2,8,35, 36]. For atomic targets (H, Li, Na, K, and Hg), a recent study [37] found well depths in good agreement, within a ratio of 1.1 to 1.2, by Li model potential with respect to $He^*(2^3S)$. Because of these findings and difficulties associated with calculations for excited states, the $Li(2^2S)$ atom was used in this study to simulate a $He^*(2^3S)$ atom. A standard 6-31+G* basis set was used, and the correlation energy correlation was partially taken into account by using second order Møller-Plesset perturbation theory (MP2). The full counterpoise method [38] was used to correct the basis set superposition errors. Natural charge

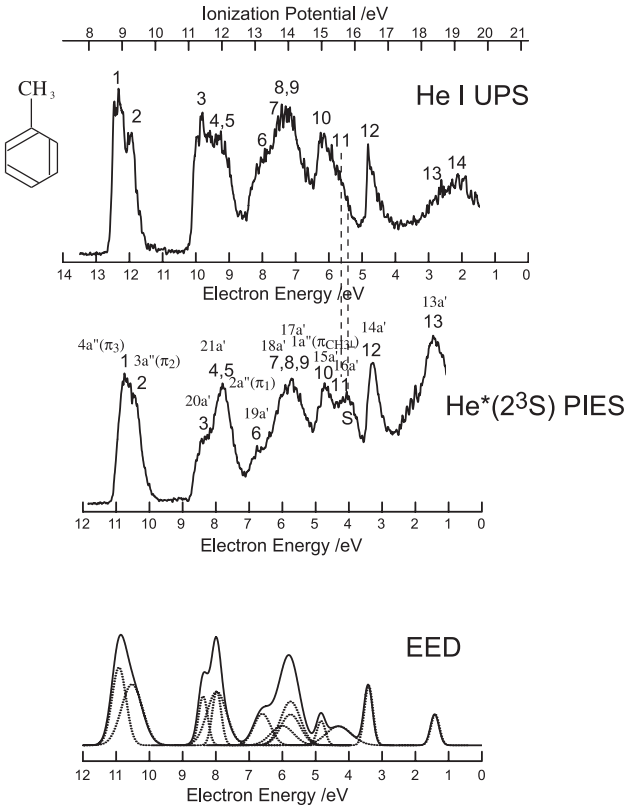

Fig. 1. He I UPS and He*(2^3S) PIES of toluene.

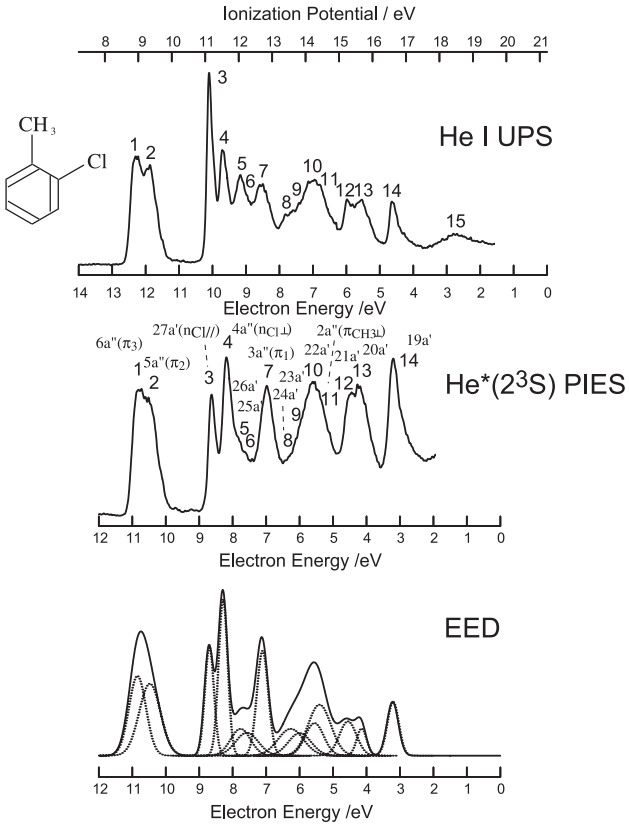

Fig. 2. He I UPS and He*(2^3S) PIES of *o*-chlorotoluene.

values for the interacting systems were calculated by natural population analysis [39] of wave functions obtained by UHF/6-311++G** calculations.

All ab initio MO calculations were carried out by utilizing a quantum chemistry program Gaussian 98 [40].

4 Results

Figures 1–3 show the He I UPS and He*(2^3S) PIES of toluene, *o*- and *p*-chlorotoluene, respectively. For an easier comparison, the electron energy scales for PIES are shifted relative to those for UPS by the difference in excitation energies, 21.22 – 19.82 eV = 1.40 eV.

Figures 4–6 show CEDPICS of toluene, *o*-, and *p*-chlorotoluene, respectively. The calculated electron density maps of MOs and simplified diagrams indicating component atomic orbitals are also plotted in the figures. Collision-energy-resolved PIES of toluene, *o*-, and *p*-chlorotoluene were shown in Figures 7–9, respectively. In each figure, the low-collision-energy spectrum is shown by a solid line and the high-collision-energy spectrum is shown by a dashed line.

Tables 1–3 summarize the vertical IPs determined by He I UPS, calculated IPs by the OVGF method, and the assignment of the observed bands. The peak energy shift (ΔE) in PIES measured with respect to the "nominal" energy E_0 (= the difference between the metastable excitation energy and the target ionization potential) are also shown in the tables. The peak energy shifts of some

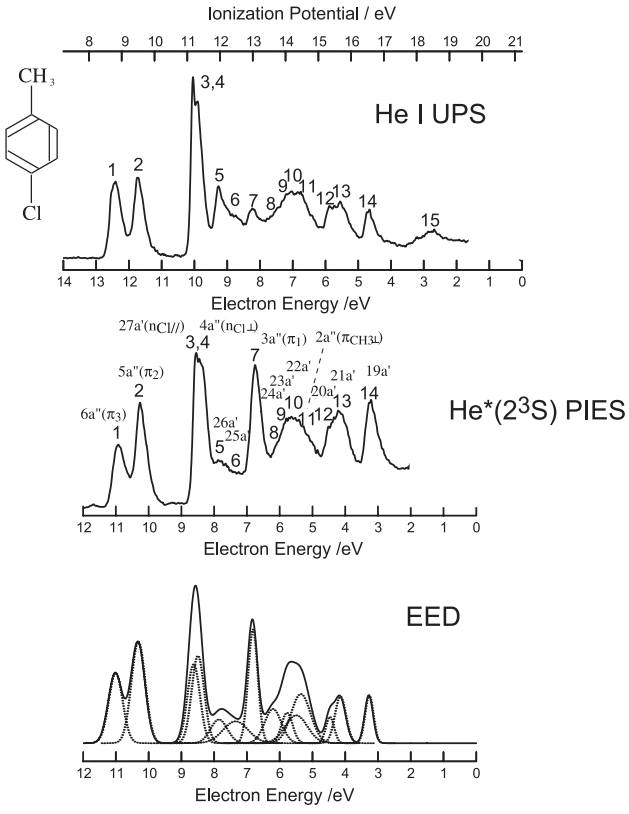

Fig. 3. He I UPS and He*(2^3S) PIES of *p*-chlorotoluene.

Table 1. Band assignments, observed IPs, calculated IPs, EED values (%), peak energy shift (ΔE) and obtained slope parameter of CEDPICS (m) for toluene.

Band	IP/eV	IP_{OVGF}/eV (pole strength)	Orbital character	EED	ΔE/meV	m
1	8.89	8.845(0.89)	$4a''(\pi_3)$	5.23	−150	−0.29
2	9.28	9.095(0.89)	$3a''(\pi_2)$	6.15	−50	−0.45
3	11.42	11.792(0.90)	$20a'^{\#1}$	2.11	-	−0.16
4	11.83	11.798(0.90)	$21a'^{\#1}$	2.33	-	−0.36
5	11.83	12.063(0.83)	$2a''(\pi_1)$	5.04	-	
6	(13.2)	13.387(0.90)	$19a'(\pi_{CH3\parallel})$	2.54	-	−0.09
7	13.80	13.775(0.88)	$18a'$	2.10	−110	−0.18
8	14.05	14.166(0.88)	$17a'^{\#1}$	2.90	-	
9	14.05	14.422(0.87)	$1a''(\pi_{CH3\perp})^{\#1}$	4.12	-	
10	14.97	15.213(0.87)	$15a'^{\#1}$	0.98	−120	−0.17
11	(15.5)	15.334 (0.87)	$16a'^{\#1}$	2.30	-	−0.35
S	(15.6)	-		-	-	
12	16.40	16.828(0.85)	$14a'$	2.40	−140	−0.14
13	(18.4)	-	$13a'$	1.25	-	−0.11
14	19.10	-	$12a'$	1.08	-	-

$^{\#1}$ Koopmans' IP order is reversed, and assigned by OVGF calculation.

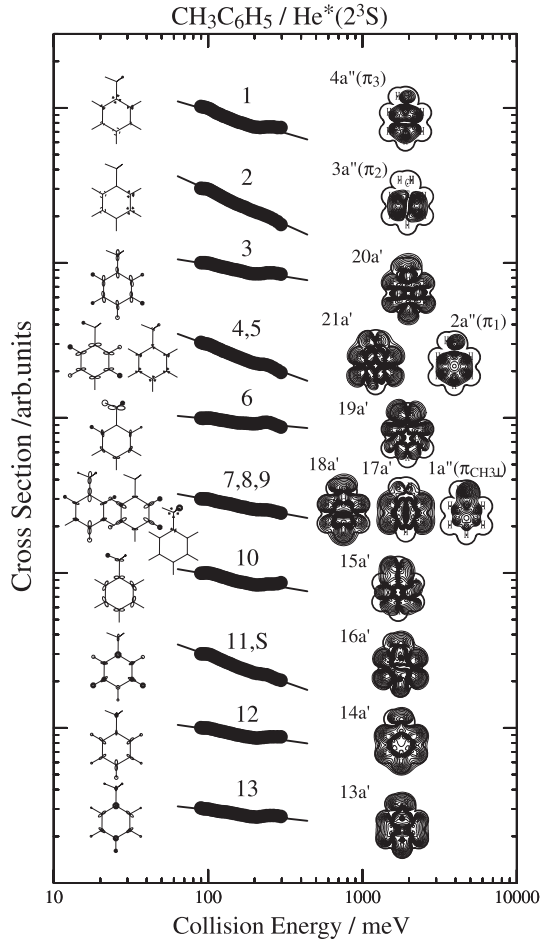

Fig. 4. Collision energy dependence of partial ionization cross-sections for toluene collided by $He^*(2^3S)$. Electron density maps of a' orbitals are plotted on the molecular plane: those of a'' orbitals are plotted on a plane above 1.7 Å from the nodal plane.

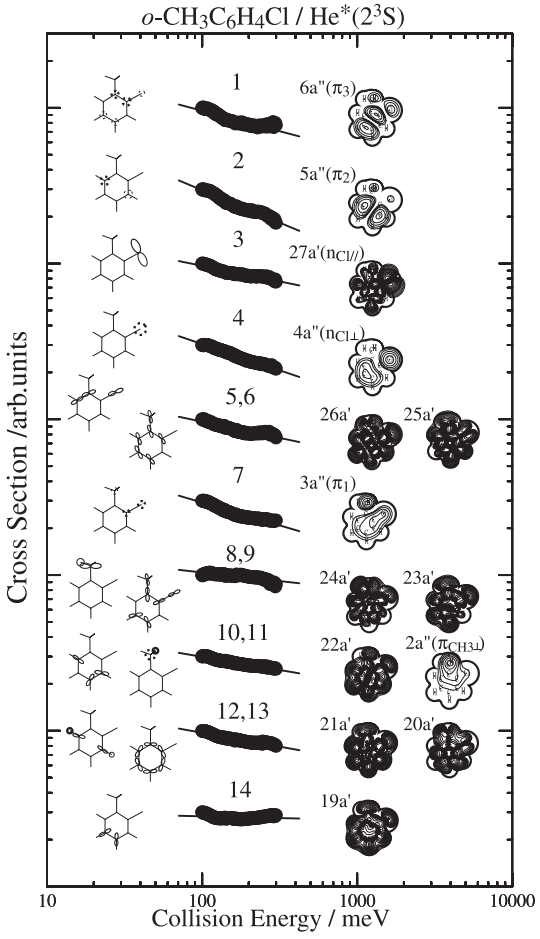

Fig. 5. Collision energy dependence of partial ionization cross-sections for *o*-chlorotoluene. Electron density maps of a' orbitals are plotted on the molecular plane: those of a'' orbitals are plotted on a plane above 1.7 Å from the nodal plane.

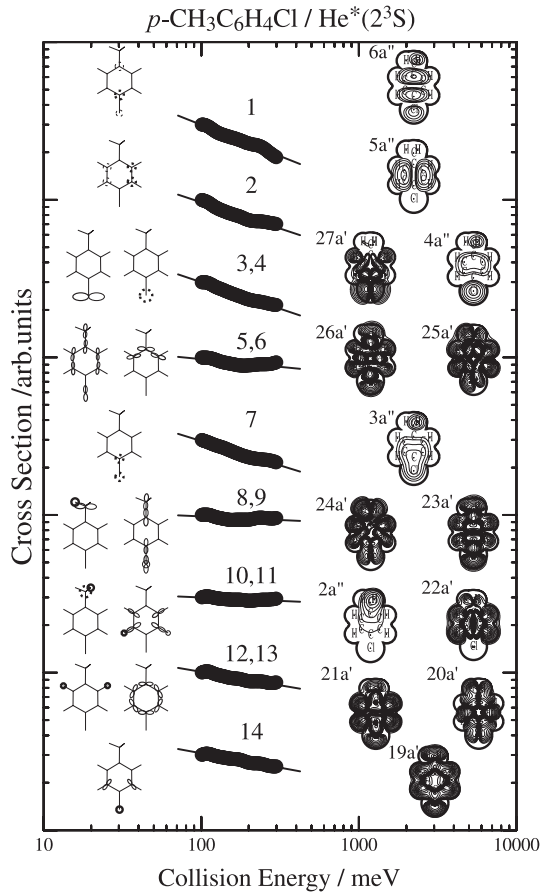

Fig. 6. Collision energy dependence of partial ionization cross-sections for *p*-chlorotoluene. Electron density maps of a' orbitals are plotted on the molecular plane: those of a'' orbitals are plotted on a plane above 1.7 Å from the nodal plane.

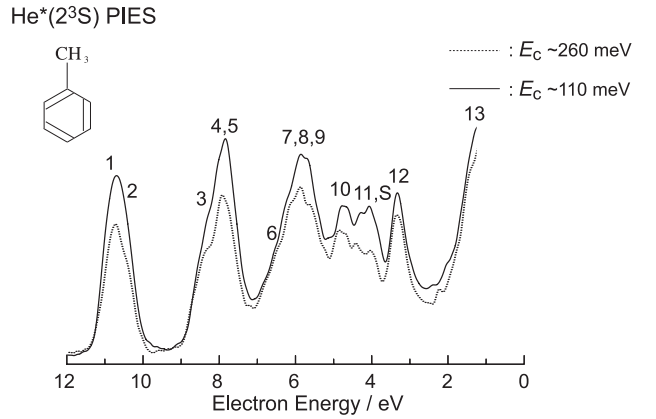

Fig. 7. $He^*(2^3S)$ collision-energy-resolved PIES of toluene: solid curve, $E_c \sim$ 249–271 meV, average 260 meV; dotted curve, $E_c \sim$ 107–114 meV, average 110 meV.

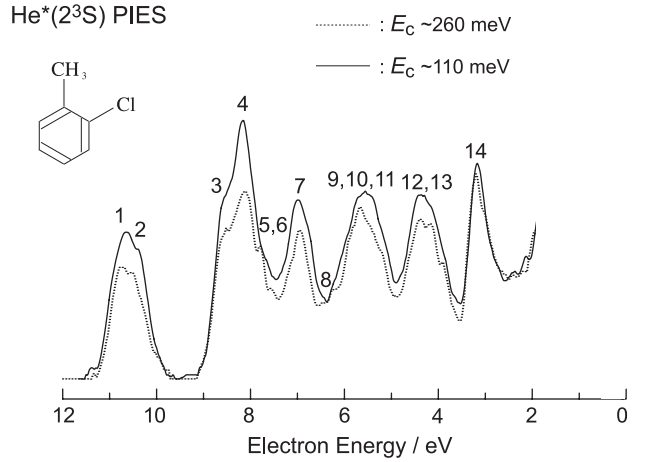

Fig. 8. $He^*(2^3S)$ collision-energy-resolved PIES of *o*-chlorotoluene: solid curve, $E_c \sim$ 249–271 meV, average 260 meV; dotted curve, $E_c \sim$ 107–114 meV, average 110 meV.

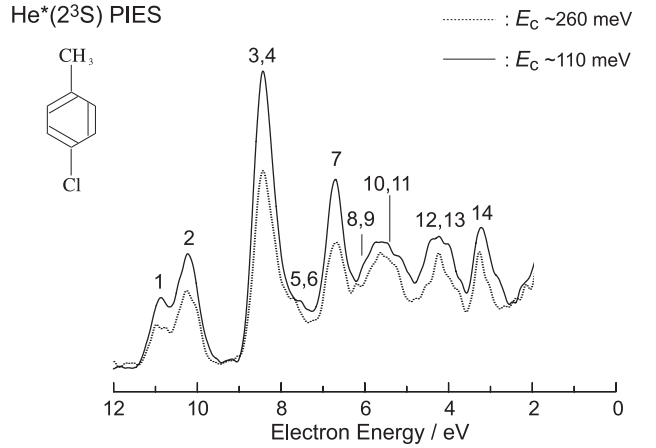

Fig. 9. $He^*(2^3S)$ collision-energy-resolved PIES of *p*-chlorotoluene: solid curve, $E_c \sim$ 249–271 meV, average 260 meV; dotted curve, $E_c \sim$ 107–114 meV, average 110 meV.

overlapping bands were not estimated. Values of the slope parameter m for the $\log\sigma$ vs. $\log E_c$ plots in collision energy range 100–300 meV were estimated by a linear least-squares method and listed in the tables.

Figure 10 shows interaction potential energy curves $V(R)$ as functions of the distance R between Li and C, Cl, or the center of the benzene ring of toluene (Fig. 10a), *o*-chlorotoluene (Fig. 10b), and *p*-chlorotoluene (Fig. 10c). Interaction potential energy curves $V(\theta)$ for Li-chlorotoluenes as functions of angle θ were shown in Figure 11 (θ is an angle from the collinear direction of the C–Cl bond axis). The angle θ was scanned on the molecular plane and the Li–Cl distance was fixed at 2.6 Å.

5 Discussion

5.1 Attractive interactions around π electrons

Since He^* atoms at smaller collision energies can be attracted to the region where the MO extends (MO region) more effectively than He^* atoms at higher collision energies, negative CEDPICS indicates attractive interactions [12,13] around the MO region. In the case of atomic

Table 2. Band assignments, observed IPs, calculated IPs, EED values (%), peak energy shift (ΔE) and obtained slope parameter of CEDPICS (m) for *o*-chlorotoluene.

Band	IP/eV	IP_{OVGF}/eV (pole strength)	Orbital character	EED	ΔE/meV	m
1	8.96	8.903(0.89)	$6a''(\pi_3)$	4.79	−80	−0.26
2	9.33	9.241(0.89)	$5a''(\pi_2)$	5.41	0	−0.42
3	11.11	11.304(0.89)	$27a'(n_{Cl\parallel})$	3.49	−80	−0.20
4	11.52	11.714(0.87)	$4a''(n_{Cl\perp})$	5.01	−130	−0.34
5	12.04	12.262(0.90)	$26a'o\sigma_{CCl})$	1.88	-	−0.21
6	12.23	12.418(0.89)	$25a'$	1.84	-	
7	12.70	12.931(0.85)	$3a''(\pi_1)$	4.20	-	−0.29
8	13.54	13.816(0.90)	$24a'(\pi_{CH3\parallel})$	2.42	-	−0.11
9	13.81	14.164(0.88)	$23a'$	1.81	-	
10	14.25	14.433(0.88)	$22a'^{\#1}$	2.12	-	−0.17
11	14.40	14.698(0.86)	$2a''(\pi_{CH3\perp})^{\#1}$	4.09	-	
12	15.25	15.643(0.87)	$21a'$	2.06	−130	−0.18
$13(S)^{\#2}$	15.66	15.810(0.87)	$20a'$	0.95	80	
14	16.60	17.026(0.85)	$19a'$	2.16	−20	−0.02
15	18.49	-	$18a'$	0.95	-	-

$^{\#1}$ Koopmans' IP order is reversed, and assigned by OVGF calculation. $^{\#2}$ Shake-up satellite band suggested by EED simulation and CEDPICS.

Table 3. Band assignments, observed IPs, calculated IPs, EED values (%), peak energy shift (ΔE) and obtained slope parameter of CEDPICS (m) for *p*-chlorotoluene.

Band	IP/eV	IP_{OVGF}/eV (pole strength)	Orbital character	EED	ΔE/meV	m
1	8.80	8.766(0.89)	$6a''(\pi_3)$	4.10	−100	−0.40
2	9.49	9.434(0.89)	$5a''(\pi_2)$	5.93	−70	−0.33
3	11.18	11.338(0.89)	$27a'(n_{Cl\parallel})$	4.15	−100	−0.34
4	11.31	11.538(0.87)	$4a''(n_{Cl\perp})$	4.60	−120	
5	11.95	12.274(0.89)	$26a'(\sigma_{CCl})$	1.66	-	−0.10
6	12.46	12.360(0.90)	$25a'$	2.30	-	
7	12.99	13.169(0.84)	$3a''(\pi_1)$	4.65	−80	−0.31
8	(13.7)	13.923(0.90)	$24a'(\pi_{CH3\parallel})$	2.40	-	−0.04
9	14.03	14.047(0.88)	$23a'$	1.42	-	
10	14.31	14.638(0.88)	$22a'^{\#1}$	2.60	-	−0.04
11	14.45	14.736(0.86)	$2a''(\pi_{CH3\perp})^{\#1}$	4.02	-	
12	15.34	15.796(0.87)	$20a'^{\#1}$	0.92	-	−0.17
$13(S)^{\#2}$	15.66	15.801(0.86)	$21a'^{\#1}$	2.17	-	
14	16.54	16.841(0.86)	$19a'$	1.68	−70	−0.18
15	18.45	-	$18a'$	1.27	-	-

$^{\#1}$ Koopmans' IP order is reversed, and assigned by OVGF calculation. $^{\#2}$ Shake-up satellite band suggested by EED simulation and CEDPICS.

targets, if the long-range attractive part of the interaction potential $V(R)$ is assumed to have a function form

$$V(R) \propto R^{-s}, \tag{3}$$

the ionization cross-section $\sigma(E_c)$ is represented [2,6] by

$$\sigma(E_c) \propto E_c^{-2/s}. \tag{4}$$

On the contrary, for repulsive interactions, Illenberger and Niehaus [6] showed that $\sigma(E_c)$ can be expressed as

$$\sigma(E_c) \propto [\ln(B/E_c)]^2 \, (E_c/B)^{(b/d)-1/2}, \tag{5}$$

based on the assumption that interaction potential $V(R)$ and the transition probability $W(R)$ can be represented by the simple expressions,

$$V(R) \propto B \exp(-dR) \tag{6}$$

and

$$W(R) \propto C \exp(-bR). \tag{7}$$

The asymptotic decay of every Hartree-Fock orbital was probed to be the same except for the Be atom and the asymptotic value of the orbital exponent was shown to be equal to $(-2\varepsilon_{HOMO})^{1/2}$, where ε_{HOMO} is the orbital energy of HOMO [41,42]. The value of b is, therefore, common for all ionic states of a given molecule M and can be expressed as

$$b = 2\,[2I(M)]^{1/2} \tag{8}$$

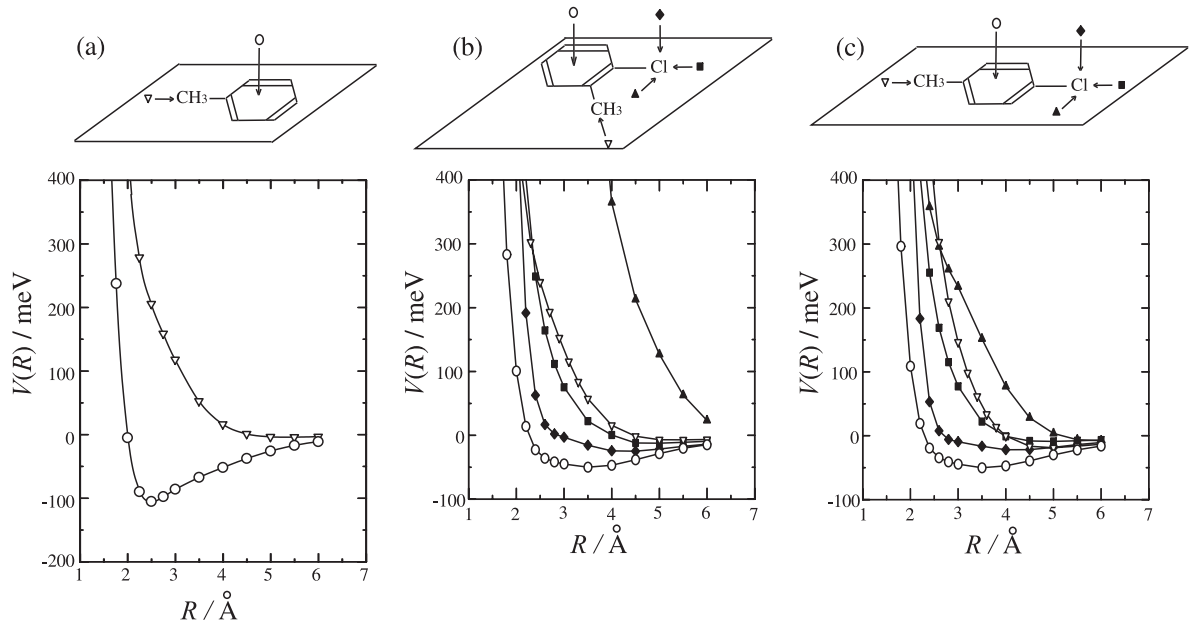

Fig. 10. Interaction potential energy curves $V(R)$ between Li and the C, Cl, or the center of the benzene ring of (a) toluene, (b) *o*-chlorotoluene, and (c) *p*-chlorotoluene.

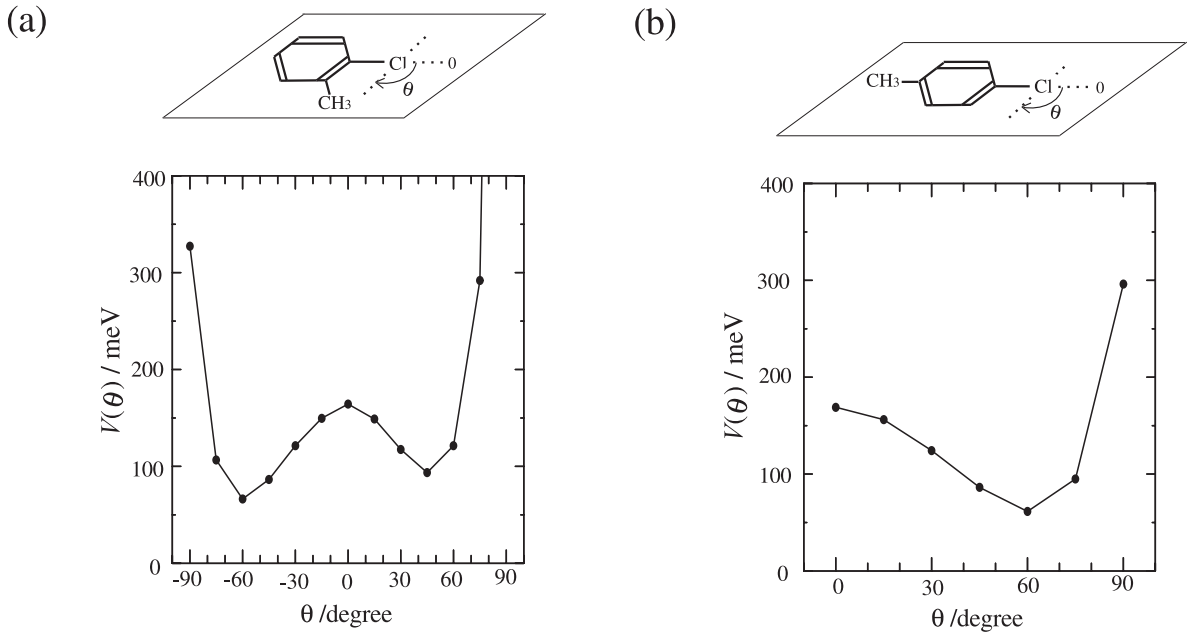

Fig. 11. Interaction potential energy curves $V(\theta)$ for (a) Li and *o*-chlorotoluene and (b) Li and *p*-chlorotoluene: θ scanning begins from the collinear direction of the C–Cl bond axis ($\theta = 0°$) with a Li–Cl distance of 2.6 Å.

where $I(M)$ is the lowest IP. Positive slope of CEDPICS shows that He* atoms at higher collision energies can access the inner reactive region against the repulsive wall with the effective hardness d $(= b/(m + 1/2))$ [13]. If the corresponding MO extends in both repulsive and attractive interaction regions, the slope value of the positive or negative CEDPICS shows the extent of deflection of incoming trajectories of He* atoms by both repulsive and attractive interactions.

For toluene, large negative slope of CEDPICS was observed for ionization from π_{1-3} orbitals distributing around the benzene ring $(-0.45 < m < -0.29)$. Attractive interaction more than 100 meV was obtained by the model potential calculation for the access of a Li atom to the center of benzene ring of toluene (Fig. 10). On the other hand, repulsive interaction was indicated for the access of a Li atom to the methyl group, and small negative slope values of CEDPICS were observed for ionization from σ

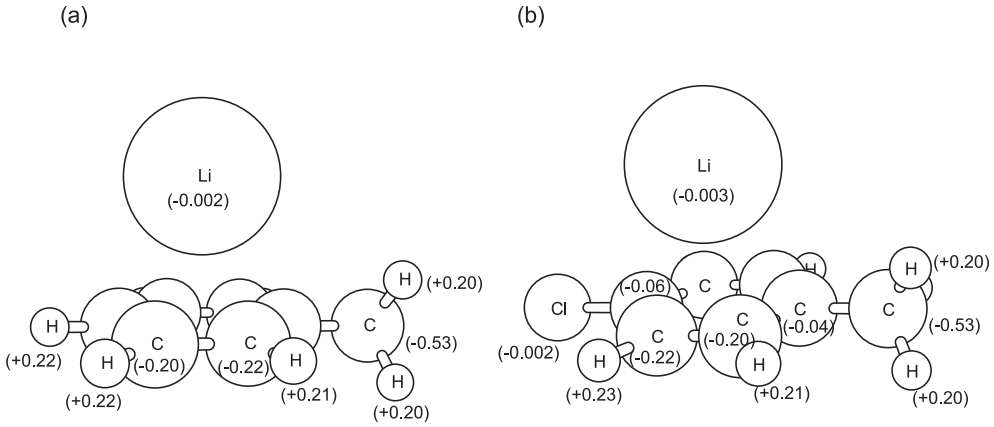

Fig. 12. Natural charge of (a) toluene–Li and (b) *p*-chlorotoluene–Li at $R = 2.5$ Å from the center of the benzene ring by natural population analysis for UHF/6-311++G** level of calculation.

or π_{CH3} orbitals except for band 11 and smaller electron energy region around 4 eV (band S). The assignment of the band S is going to be discussed in Section 5.3.

For *p*- and *o*-chlorotoluenes, similar negative slope values of CEDPICS with those for toluene were observed for ionization from π_{1-3} orbitals. Although the first two π bands of toluene and *o*-chlorotoluene overlap largely in PIES, negative slope value of CEDPICS for band 1 results to be smaller than that of band 2, which can be caused by the repulsive interaction around the methyl group in ionization from the π_3 orbital. The negative slope value of CEDPICS for the band 1 of *p*-chlorotoluene is, however, relatively large ($m = -0.40$). In a comparison with toluene, substitution effect was reflected in the negative CEDPICS for band 1. For the case of benzene [20,21], the negative slope value of π_1 band is similar to that for ionization from degenerate $\pi_{2,3}$ orbitals ($m \sim -0.3$), while the largest negative slope values of CEDPICS for π bands of toluene and *p*- and *o*-chlorotoluenes are more than –0.40 and the in-phase extending of π_1 orbital at the center position of the benzene ring does not result in the largest negative slope of CEDPICS. This can be ascribed to the complex interaction potential surface for the out-of-plane direction of the studied molecules by the substitution.

Interaction potential calculations (Fig. 10) indicate that substitution of an H atom in benzene ring of toluene with a Cl atom (chlorotoluene) has an influence on the attractive interaction for out-of-plane direction above the ring. In the case of toluene, interaction potential is attractive with value of –105 meV at the distance $R = 2.5$ Å from the center of the ring, while the energy value increased to –35 meV at $R = 3.5$ Å (–16 meV at $R = 2.5$ Å) for *p*-chlorotoluene and –34 meV at $R = 3.5$ Å (–12 meV at $R = 2.5$ Å) for *o*-chlorotoluene. Natural charge values by natural population analysis of UHF/6-311++G** calculations was shown in Figure 12 for toluene–Li and *p*-chlorotoluene–Li at $R = 2.5$ Å. One can find that positive charge values of H atoms ($\sim$+ 0.2) in the ring for toluene–Li are quite different from the slight negative charge on the Cl atom (-0.002) of *p*-chlorotoluene–Li. This difference can be caused by the larger electronegativity of a Cl atom (+ 3.0) rather than an H atom (+2.1) [32].

Interesting checking of the electronegativity effect has been performed in interaction potential calculations for 2,4,6-trichlorotoluene–Li and *p*-fluorotoluene–Li. The obtained calculation results for 2,4,6-trichlorotoluene–Li are effected by repulsive interaction with the energy values of –4.4 meV at $R = 3.5$ Å and +128 meV at $R = 2.5$ Å. For the case of *p*-fluorotoluene–Li, the large electronegativity of an F atom (+4.0) results in relatively smaller attractive interaction with the values of –22 meV at $R = 3.5$ Å (+30 meV at $R = 2.5$ Å) compared with the case of *p*-chlorotoluene–Li. Although obtained slope parameters of CEDPICS for ionization from π orbitals of toluene ($m = -0.37$ in average) were not different largely from those of *o*-chlorotoluene ($m = -0.34$ in average) and *p*-chlorotoluene ($m = -0.35$ in average), observation of the electronegativity effect on the CEDPICS of π bands by the substitution groups can be expected for *p*-fluorotoluene or 2,4,6-trichlorotoluene. It should be noted that a previous study indicates smaller negative slope of CEDPICS for π bands of fluorobenzenes such as 1,3,5-triflorobenzne ($m = -0.22$ in average) [43] rather than benzene ($m = -0.30$ in average) [21].

5.2 Anisotropic interactions around C–Cl bonds

Attractive interactions around the C–Cl bonds were suggested by the negative slope of CEDPICS for ionization from nonbonding chlorine orbitals distributing to out-of-plane direction ($n_{Cl\perp}$) of *o*-chlorotoluene. Small attractive interaction potential with the well depth of $\sim$30 meV was indicated by the model potential calculation for out-of-plane approaching of He* to the Cl atom (Fig. 10). In the case of a sulfur atom, attractive interaction was found for the vertical direction of C–S or C=S bonds [44–46] similarly with the C–Cl case. This is reversed trend with C=O (Refs. [45,46]) or C–F (Refs. [24,43]) case depending on the period of chalcogen or halogen atoms, where collinear direction is the most attractive direction for the case of C=O and C–F bonds.

For in-plane direction, relatively smaller negative slope value of CEPICS for ionization from $n_{\mathrm{Cl}\parallel}$ orbital of *o*-chlorotoluene ($m = -0.20$) than that of $n_{\mathrm{Cl}\perp}$ orbital ($m = -0.34$) was observed, which is consistent with the repulsive interaction effect of the shielding effect by the methyl group and H atoms in model potential calculation (Figs. 10 and 11). Due to the overlapping of $n_{\mathrm{Cl}\parallel}$ and $n_{\mathrm{Cl}\perp}$ bands, difference in slope of CEDPICS was not able to be observed. As for the collinear approaching to the C–Cl bonds, repulsive interaction was obtained by the model potential calculation. Although ionization band from σ_{CCl} ($26a'$) orbitals can be assigned to band 5 for *p*- and *o*-chlorotoluenes, band 6 ionized from $25a'$ σ_{CC} orbitals is overlapping with band 5. Obtained slope values of CEDPICS for bands 5,6 are small negative, and the model potential calculation resulted in repulsive or very weak attractive interaction with well depth of ∼10 meV. For the case of chlorobenzene [24], small negative slope value of CEDPICS was obtained ($m = -0.17$).

The well depth of attractive interaction can be estimated by the negative peak energy shift values (ΔE) if the potential energy in exit channel is assumed to be flat. The obtained peak energy shift values for ionization from the Cl lone-pair orbitals are around –100 meV, which was relatively larger values than obtained well depth by model potential calculations (ca. –25 meV). This inconsistency may be ascribed to insufficient electron correlation effect, limit of model potential calculations, and repulsive exit potential curves.

5.3 EED spectra and shake-up band observed in PIES

He I UPS and $\mathrm{He}^*(2^3\mathrm{S})$ PIES of halogenotoluenes were measured, and all observed bands in UPS of chlorotoluenes were assigned to MOs based on band intensity in PIES and SCF calculations [25]. However, there are some inconsistency for the band assignment between IP orders based on Koopmans' theorem and OVGF calculations in this study.

As for toluene, OVGF calculation results in nearly degenerate ionic states for ionization from $20a'$ and $21a'$ orbitals, while EED simulation of PIES reproduced weak intensity of band 3 and strong bands 4,5. Since EED values and orbital character for $21a'$ and $20a'$ orbitals is similar, assignment of band 3 cannot be determined by PIES and CEDPICS. Overlapping bands 7–9 are also difficult to assign to orbitals. Negative slope of CEDPICS for band 11,S is steep ($m = -0.35$), which can be ascribed to a $\pi^{-2}\pi^{*+1}$ shake-up satellite state because of the similar negative slope value of CEDPICS with that of π bands. In the case of benzene, $\pi^{-2}\pi^{*+1}$ shake-up satellite band was observed around 3.5 eV in electron energy [15,21,47] and negative slope of CEDPICS ($m \sim -0.21$) was obtained [21]. Another proof of the S band is small EED value for $16a'$ orbital (2.30) which is similar value with EED for $19a'$ (band 6).

For the case of chlorotoluenes, assignment of bands 10,11 can be reversed with Koopmans' IP order because of the OVGF results. Since EED simulations of PIES with Koopmans's IP order and OVGF IP order resulted in slight difference in bands 10,11, the assignment of bands 10,11 was not able to determine. The relatively large negative slope of CEDPICS for band 10,11 of *o*-chlorotoluene can be ascribed to the electron density for out-of-plane direction around the Cl atom of $2a''$ orbital. On the other hand, negative slope of CEDPICS and large intensity for bands 12,13 of *p*- and *o*-chlorotoluene cannot be explained by electron density distribution. Shake-up satellite being similar with toluene may exist under the direct ionization bands of *p*- and *o*-chlorotoluene. EED simulation of bands 12,13 with OVGF IP order for *p*-chlorotoluene gives better agreement with observed PIES than Koopmans' IP order.

Different negative slope of CEDPICS for band 14 of *p*-chlorotoluene ($m = -0.18$) and *o*-chlorotoluene ($m = -0.02$) for ionization from $19a'$ MO that is the in-phase σ_{CH} orbital outside the molecular surface is interesting, which may be ascribed to larger Cl component of $19a'$ MO in *p*-chlorotoluene rather than that of *o*-chlorotoluene.

6 Conclusion

We have reported on the two-dimensional collision-energy-resolved PIES study of stereodynamics in collisional ionization of toluene and *o*, *p*-chlorotoluenes with $\mathrm{He}^*(2^3\mathrm{S})$ metastable atoms in conjunction with outer-valence Greens' function (OVGF) calculation for ionization potential energies as well as exterior electron density (EED) calculation of partial ionization cross-sections in Penning ionization. Negative collision energy dependence of partial ionization cross-sections (CEDPICS) for ionization band observed at ca. 4 eV in electron energy can be ascribed to $\pi^{-2}\pi^{*+1}$ shake-up satellite band, which is also supported by inconsistency in observed PIES and EED simulation of direct Penning ionization. Assignments of ionization bands were examined by OVGF and EED calculations based on the ionization potential order by Koopman's theorem.

Anisotropic interaction and stereodynamics in the collisional ionization have relation with the substitution of an H atom in benzene ring of toluene with a Cl atom. Observation of CEDPICS indicates that the difference in stereodynamics for ionization from Cl lone-pair orbitals of *o*− and *p*-chlorotoluenes is caused by the shielding effect for in-plane directions by the methyl group. For out-of-plane direction, interaction potential calculations for the access of He^* to the π orbital region show attractive interaction for toluene rather than chlorotoluenes due to large electronegativity of the Cl atom.

This work has been supported by a Grant in Aid for Scientific Research from the Japanese MEXT (Ministry of Education, Culture, Sports, Science and Technology) and JSPS (Japan Society for the Promotion of Science).

References

1. F.M. Penning, Naturwissenschaften **15**, 818 (1927)
2. A. Niehaus, Adv. Chem. Phys. **45**, 399 (1981)

3. P.E. Siska, Rev. Mod. Phys. **65**, 337 (1993)
4. V. Čermák, J. Chem. Phys. **44**, 3781 (1966)
5. A.J. Yencha, *Electron Spectroscopy: Theory, Technique, and Application*, edited by C.R. Brundle, A.D. Baker, (Academic, New York, 1984), Vol. 5
6. E. Illenberger, A. Niehaus, Z. Phys. B **20**, 33 (1975)
7. J.P. Riola, J.S. Howard, R.D. Rundel, R.F. Stebbings, J. Phys. B **7**, 376 (1974)
8. W. Lindinger, A.L. Schmeltekopf, F.C. Fehsenfeld, J. Chem. Phys. **61**, 2890 (1974)
9. M.R. Woodard, R.C. Sharp, M. Seely, E.E. Mushlitz Jr, J. Chem. Phys. **69**, 2978 (1978)
10. T.P. Parr, D.M. Parr, R.M. Martin, J. Chem. Phys. **76**, 316 (1982)
11. L. Appolloni, B. Brunetti, J. Hermanussen, F. Vecchiocattivi, G.G. Volpi, J. Chem. Phys. **87**, 3804 (1987)
12. K. Mitsuke, T. Takami, K. Ohno, J. Chem. Phys. **91**, 1618 (1989)
13. K. Ohno, T. Takami, K. Mitsuke, T. Ishida, J. Chem. Phys. **94**, 2675 (1991)
14. D.C. Dunlavy, D.W. Martin, P.E. Siska, J. Chem. Phys. **93**, 5347 (1990)
15. T. Takami, K. Ohno, J. Chem. Phys. **96**, 6523 (1992)
16. K. Ohno, H. Yamakado, T. Yamata, T. Ogawa, J. Chem. Phys. **105**, 7536 (1995)
17. H. Hotop, A. Niehaus, Z. Phys. **228**, 68 (1969)
18. K. Ohno, H. Mutoh, Y. Harada, J. Am. Chem. Soc. **105**, 4555 (1983)
19. K. Ohno, K. Imai, S. Matsumoto, Y. Harada, J. Chem. Phys. **81**, 4447 (1984)
20. Y. Yamakita, M. Yamauchi, K. Ohno, Chem. Phys. Lett. **332**, 189 (2000)
21. M. Yamazaki, S. Maeda, N. Kishimoto, K. Ohno, J. Chem. Phys. **122**, 044303 (2005)
22. N. Kishimoto, K. Ohshimo, K. Ohno, J. Electron Spectrosc. Relat. Phenom. **104**, 145 (1999)
23. K. Imura, N. Kishimoto, K. Ohno, J. Phys. Chem. A **105**, 6378 (2001)
24. K. Imura, N. Kishimoto, K. Ohno, J. Phys. Chem. A **105**, 4189 (2001)
25. S. Fujisawa, I. Oonishi, S. Masuda, K. Ohno, Y. Harada, J. Phys. Chem. **95**, 5742 (1991)
26. T. Takami, K. Mitsuke, K. Ohno, J. Chem. Phys. **95**, 918 (1991)
27. K. Ohno, Bull. Chem. Soc. Jpn **77**, 887 (2004)
28. J.L. Gardner, J.A.R. Samson, J. Electron Spectrosc. Rel. Phen. **8**, 469 (1976)
29. K. Kimura, S. Katsumata, Y. Achiba, T. Yamazaki, S. Iwata, *Handbook of He I Photoelectron Spectra of Fundamental Organic Molecules* (Japan Scientific Press, Tokyo, 1981)
30. N. Kishimoto, J. Aizawa, H. Yamakado, K. Ohno, J. Phys. Chem. A **101**, 5038 (1997)
31. A.D. Becke, J. Chem. Phys. **98**, 5648 (1993); C. Lee, W. Yang, R.G. Parr, Phys. Rev. B **37**, 785 (1988)
32. L. Paling, *The Nature of the Chemical Bond* (Cornell University, Ithaca, NY, 1960)
33. L.S. Cederbaum, W. Domcke, Adv. Chem. Phys. **36**, 205 (1977); W. von Niessen, J. Schirmer, L.S. Cederbaum, Comp. Phys. Rep. **1**, 57 (1984); J.V. Ortiz, J. Chem. Phys. **89**, 6348 (1988); V.G. Zakrzewski, W. von Niessen, J. Comp. Chem. **14**, 13 (1993)
34. E.W. Rothe, R.H. Neynaber, S.M. Trujillo, J. Chem. Phys. **42**, 3310 (1965)
35. H. Hotop, Radiat. Res. **59**, 379 (1974)
36. H. Harberland, Y.T. Lee, P.E. Siska, Adv. Chem. Phys. **45**, 487 (1981)
37. H. Hotop, T.E. Roth, M.-W. Ruf, A.J. Yencha, Theor. Chem. Acc. **100**, 36 (1998)
38. S.F. Boys, F. Bernardi, Mol. Phys. **19**, 553 (1970)
39. A.E. Reed, R.B. Weinstock, F. Weinhold, J. Chem. Phys. **83**, 735 (1985)
40. M.J. Frisch et al., *Gaussian 98*, Revision A.9 (Gaussian Inc., Pittsburgh, PA, 1998)
41. N.C. Handy, M.T. Marron, H.J. Silverstone, Phys. Rev. **180**, 45 (1969)
42. M.M. Morrell, R.G. Parr, M. Levy, J. Chem. Phys. **62**, 549 (1975)
43. K. Imura, N. Kishimoto, K. Ohno, J. Phys. Chem. A **105**, 10781 (2001)
44. N. Kishimoto, R. Yokoi, H. Yamakado, K. Ohno, J. Phys. Chem. A **101**, 3284 (1997)
45. N. Kishimoto, Y. Osada, K. Ohno, J. Phys. Chem. A **104**, 1393 (2000)
46. N. Kishimoto, Y. Osada, K. Ohno, J. Electron Spectrosc. Rel. Phen. **114-116**, 183 (2001)
47. S. Masuda, M. Aoyama, K. Ohno, Y. Harada, Phys. Rev. Lett. **65**, 3257(1990)